Erschienen in: APL Materials ; 4 (2016), 9. - 091901
https://dx.doi.org/10.1063/1.4960759

APL MATERIALS **4**, 091901 (2016)

Characterization of perovskite solar cells: Towards a reliable measurement protocol

Eugen Zimmermann,[1] Ka Kan Wong,[1] Michael Müller,[1] Hao Hu,[1] Philipp Ehrenreich,[1] Markus Kohlstädt,[2,3] Uli Würfel,[2,3] Simone Mastroianni,[2] Gayathri Mathiazhagan,[2] Andreas Hinsch,[2] Tanaji P. Gujar,[4] Mukundan Thelakkat,[4] Thomas Pfadler,[1] and Lukas Schmidt-Mende[1]
[1]*Department of Physics, University of Konstanz, 78457 Konstanz, Germany*
[2]*Fraunhofer Institute for Solar Energy Systems ISE, Heidenhofstr. 2, 79110 Freiburg, Germany*
[3]*Freiburg Materials Research Center FMF, University of Freiburg, Stefan-Meier-Str. 21, 79104 Freiburg, Germany*
[4]*Applied Functional Polymers, Department of Macromolecular Chemistry I, University of Bayreuth, 95440 Bayreuth, Germany*

(Received 28 June 2016; accepted 27 July 2016; published online 19 August 2016)

Lead halide perovskite solar cells have shown a tremendous rise in power conversion efficiency with reported record efficiencies of over 20% making this material very promising as a low cost alternative to conventional inorganic solar cells. However, due to a differently severe "hysteretic" behaviour during current density-voltage measurements, which strongly depends on scan rate, device and measurement history, preparation method, device architecture, etc., commonly used solar cell measurements do not give reliable or even reproducible results. For the aspect of commercialization and the possibility to compare results of different devices among different laboratories, it is necessary to establish a measurement protocol which gives reproducible results. Therefore, we compare device characteristics derived from standard current density-voltage measurements with stabilized values obtained from an adaptive tracking of the maximum power point and the open circuit voltage as well as characteristics extracted from time resolved current density-voltage measurements. Our results provide insight into the challenges of a correct determination of device performance and propose a measurement protocol for a reliable characterisation which is easy to implement and has been tested on varying perovskite solar cells fabricated in different laboratories. [http://dx.doi.org/10.1063/1.4960759]

Over the last seven years, the rise of organic-inorganic metal halide perovskites, like $CH_3NH_3PbI_3$, has led to significant change in research direction of the whole hybrid photovoltaic community. Starting with power conversion efficiencies of 3.81% in 2009,[1] fabricated devices made a huge leap to about 10% in 2012,[2–4] and have improved rapidly to the highest reported values for hybrid photovoltaics of over 20%.[5] Many groups all over the world adapted their specialized knowledge of optimized fabrication and characterization techniques of hybrid and organic solar cells (i.e., DSSCs, BHJ SCs, electrodes, etc.) to contribute to this tremendous rise. Along with this unprecedented development, many different challenges have been revealed such as long term stability,[6] the replacement of the toxic Pb, a highly reproducible large scale fabrication process of the active layer,[7–9] and a "hysteretic" behaviour of fabricated solar cells during current density-voltage (J-V)-characterization.[10,11] While long term stability probably can be achieved by device encapsulation as for common organic and dye sensitized photovoltaics,[12] the active layer fabrication issues have been successfully addressed by various approaches like different deposition techniques,[13–15] solvent engineering procedures,[16] pre- and post-treatments,[17,18] and an appropriate choice of the underlying substrate layer.[19,20] Among this, the hysteretic behaviour has been studied

intensively, revealing strong indications for ion migration as the dominating origin.[10,11,21] This leads to a build-up of space charges at the interface and results in a scan rate and settle condition dependent photocurrent extraction probability.[11] Nevertheless, many other possible origins like a morphological change, a ferroelectric polarization by the rotating methylammonia cations, capacitive charge accumulation/space charges, trapping and detrapping of charges, chemical degradation, light-doping, and photo induced ion migration[10,11,22–29] can simultaneously contribute to or enhance this behaviour. Moreover, occurring processes and related time scales differ for different architectures (flat vs. structured), varying material combinations, electrodes, illumination conditions, and scan parameters. This makes a final conclusion about the origin of the hysteresis in perovskite solar cells (PSCs) and how to deal with it during device characterization difficult, even though specific characterization procedures have been elaborated.[11] Hence, an increasing number of publications demonstrate (almost) hysteresis free cells whereas a TiO_2 free device geometry, utilizing, e.g., PEDOT:PSS as hole transport layer (HTL) and C_{60}/PCBM as electron transport layer (ETL) turns out to be particularly successful.[30–33]

While some of the already existing measurement procedures reduce the hysteresis effect and result in matching results for forward and reverse scan directions, these specific approaches might neglect some of the underlying processes or do not represent steady state working conditions. In particular, very fast scan rates, which are suggested to limit the cell response to the electronic properties, are not related to a stabilized power output anymore and can lead to relative deviations between different scan directions and scan speeds of up to 50% or even more by additionally adjusting prior settle conditions.[11,22,34] Furthermore, the introduction of a hysteresis factor/index which represents the difference of the J-V curve at a certain voltage ($0.8^{*}V_{OC}$) for both scan directions is questionable[23,35] since the hysteresis is highly dependent on measurement conditions, which in turn will strongly influence this hysteresis factor. Also, calculation of an average J-V curve or particular characteristics, determined from different scan directions and scan speeds, does not represent real device characteristics and should be avoided due to the aforementioned reasons. Finally, even a comparison of measured J_{SC} values to the calculated values obtained from external quantum efficiency (EQE) measurements is challenging as these measurements depend on a combination of light bias intensity and chopping frequency.[36]

Some of these issues have been already discussed in preceding publications (see Refs. 10, 22, 28, and 34) and point out the challenges of acquiring reasonable data. In this work we want to summarize the challenges of achieving a detailed and reliable picture of the ongoing processes during a J-V-characterization and propose a measurement protocol for reproducible and comparable results as an extension to the existing ISOS-protocols for organic solar cells.[37] This new measurement protocol is tested for various device architectures and geometries and includes an adaptive tracking of the maximum power point (MPP), the open circuit voltage (V_{OC}), and the short circuit current (J_{SC}), as well as cyclic and time resolved J-V-measurements. Corresponding Matlab code with all functions implemented can be found at GitHub.[38]

For perovskite solar cells a qualitative characterization by a standard J-V measurement is helpful for a brief glance whether fabricated solar cells are working or not. However, since efficiency and all other derived parameters like J_{SC}, V_{OC}, FF, as well as shunt (R_{SC}) and series (R_S) resistance depend on the severity of hysteretic behaviour and specific scan and settle parameters, a transient maximum power point (MPP) tracking should be included into any representative measurement protocol. This gives a comparable stabilized power conversion efficiency $\eta = \frac{P_{MPP}}{P_{in}}$ at working conditions as already proposed by other groups.[10,22,39] We suggest adding MPP tracking as the initial measurement with a duration of at least 60 s, which can improve comparability in several ways. First, tracking of the maximum power point stabilizes the solar cell and returns the real power output under working conditions, which is independent of measurement conditions as settle voltage and sweep rate. Furthermore, it demonstrates the stability of the cell over time, and reveals effects like beneficial light soaking or degradation. Finally, it sets a defined protocol for the first measurement and prevents arbitrary settle conditions (i.e., light soaking time, settle bias) prior to measurement. This easily can be extended to an additional tracking of the J_{SC} and the V_{OC} leading to comparable and hysteresis free device characteristics.

Further details on the ongoing processes and their respective time scales can be gained by a time resolved J-V measurement (step wise J-V measurement,[22] time resolved staircase voltammetry measurements[28]). Thereby, the current is monitored as a function of time for each individual voltage step. Among the reconstruction of the regular J-V curve, acquired data allow the extraction of involved time constants by fitting an appropriate function, and the estimation of charge flow by integration of each individual voltage step.[28] Simultaneously, extracted relaxation times can be used for determination of the steady state condition, and implemented as time delay in J-V measurements.

In order to prove steady state conditions for time constants obtained in time resolved J-V measurement, a cyclic J-V measurement can provide sufficient insight. Compared to regular J-V measurements, cyclic measurements start from the maximum power point (best extracted from MPP tracking) with a following closed sweep to J_{SC}, V_{OC}, and back to J_{SC}. This closed loop again sets a defined starting point and eliminates arbitrary delays and settle points between different scan directions. Additionally, a smooth transition between scan directions avoids an initial huge voltage step in particular for the scan in reverse direction which for certain cell geometries results in long relaxation times in the range of tens of seconds.

In contrast to time resolved J-V measurement, a transient current measurement at a fixed voltage point allows a much better determination of long term processes on the time scale of minutes. Extracted time constants can be compared to values from time resolved sweeps, however, additional time constants can be observed for various cell geometries which are exceeding practical time scales for time resolved J-V measurements since they are in the range of minutes. While this is a helpful tool to investigate long term processes, these information are not necessary for general performance measurements.

In order to demonstrate the advantage of these measurement techniques in a fixed characterization procedure, measurements have been performed on perovskite devices prepared in different laboratories with varying device architectures, preparation methods, and material combinations. These devices show pronounced differences in their hysteretic behaviour due to widely differing relaxation time scales, and thus, lead to individual requirements for appropriate hysteresis free measurements. In addition, the developed measurement procedure was applied to an organic solar cell[40] to demonstrate a hysteresis free system, which does not require such an extended measurement protocol.

The performed measurement protocol is listed in Table I, consisting of a J-V measurement (I) in forward and reverse scan direction with standard measurement conditions commonly used for organic and hybrid solar cells, which is extended by a tracking of the maximum power point, the J_{SC}, and the V_{OC} (II). Additionally, the degree of hysteretic behaviour was investigated by a cyclic (III) and a time resolved (IV) J-V measurement (see Figures S3 and S4 of the supplementary material). Finally, a second standard J-V measurement (V) with the same parameters as in (I) was performed for direct comparison to the initial curves. Due to the technical implementation, measurements marked by an asterisk consist of an additional J-V measurement (as in I.a.) for the extraction of MPP and V_{OC} as start parameters.

Results for solar cell devices measured with this protocol are shown in Figure 1, Figure S3, and Figure S4, whereas Table II gives a comprehensive summary of device characteristics for measurements I, II, and V, as well as the extracted values from reconstructed J-V curves of IV. In order to avoid uncontrolled influences by varying ambient conditions, all measurements have been performed in a glovebox under nitrogen atmosphere. A comparison to measurements under ambient conditions is shown in Figures S1 and S2, and Table S1 of the supplementary material.

For all measured cells, scan parameters were kept fixed at same not optimised values, demonstrating a highly differing hysteretic behaviour among the investigated device architectures. Thereby, device characteristics derived from J-V measurements can significantly deviate from stabilized values of maximum power point, J_{SC}, and V_{OC}, which are tracked for 60 s (see Figure 1). For stable devices, tracking of device characteristics can be prolonged up to 30 min and beyond (see Figure S2 of the supplementary material). This, however, requires an elevated degree of stability of fabricated solar cells encouraging a more stability focused research direction, which is also in line with commercialization aspects. It has the additional advantage that cells reported with this protocol have passed this initial stress test.

TABLE I. All performed measurements in consecutive order. Measurements without detailed conditions are performed as measurement I. Measurements marked by an asterisk consist of a preceding J-V measurement (I.a.) for extraction of start values of MPP and V_{OC}.

I. Standard J-V measurement[a]
a. → forward
b. ← reverse
II. Steady state tracking[b,*]
a. Maximum power point
b. J_{SC}
c. V_{OC}
III. Cyclic J-V measurement[c,*] (optional)
a. MPP → J_{SC} → V_{OC} → J_{SC}
IV. Time resolved J-V measurement (optional)
a. → forward
b. ← reverse
V. Standard J-V measurement (optional)
a. → forward
b. ← reverse

[a]Sweep from 0 to 1 V, 10 mV step size, 10 ms delay time, 5 s settle time at starting point.
[b]60 s each.
[c]50 mV step size, 10 s per step.

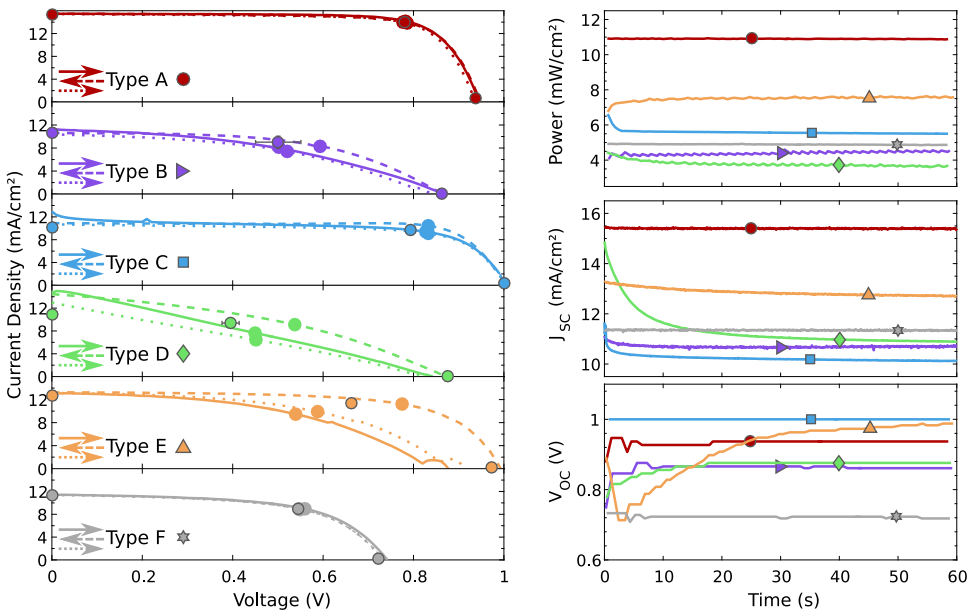

FIG. 1. (Left) Consecutive J-V measurements with fixed scan parameters (see Table I) in forward, reverse, and forward scan directions. The corresponding maximum power points are marked with a colored dot. (Right) Tracking of maximum power point, J_{SC}, and V_{OC} as a function of time. The corresponding steady state values (dark border) shown in (left) are calculated as a mean value from the last 50% of corresponding data curves in (right). Symbols in (right) are introduced for easier assignment and just represent the respective device. Device types are (A) ITO/PEDOT : PSS/$CH_3NH_3PbI_{3-x}Cl_x$/C_{60}/LiF/Ag, (B) FTO/c-TiO_2/PCBM/$CH_3NH_3PbI_3$/P3HT/WO_3/Ag, (C) ITO/PEDOT : PSS/$CH_3NH_3PbI_3$/PCBM/Ba/Ag, (D) FTO/c-TiO_2/mp-TiO_2/mp-Al_2O_2/$CH_3NH_3PbI_3$/Graphite, (E) FTO/c-TiO_2/mp-TiO_2/$CH_3NH_3PbI_3$/spiro-OMeTAD/WO_3/Ag, (F) ITO/TiO_2/BCP/PTB7:PCBM/PEDOT:PSS/Ag.

TABLE II. Comprehensive summary of solar cell characteristics of all types of investigated devices. Devices of Type A, B, C, E, and F have been measured at 82 mA/cm^2, whereas Type C and D were measured at 100 mW/cm^2 light intensity. Steady state values are shown in bold.

		Measurement							
		I.a	I.b	II.a	II.b	IV.a	IV.b	V.a	V.b
Device		→	←	→	•	→	←	→	←
Type A (○)	PCE	13.52	13.68	13.52	**13.56**	13.14	12.89	12.77	12.54
ITO/PEDOT:PSS/Perovskite/	FF	75.62	76.17	76.19	**77.25**	75.54	75.05	74.63	73.02
C_{60}/LiF/Ag	J_{SC}	15.34	15.36	15.35	**15.26**	15.16	14.93	14.92	14.95
	V_{OC}	0.96	0.97	0.96	**0.95**	0.95	0.95	0.95	0.95
Type B (▷)	PCE	4.92	6.00	4.66	**5.41**	5.65	5.44	4.94	6.00
FTO/c-TiO_2/PCBM/	FF	41.42	54.04	43.53	**48.46**	51.26	52.05	55.00	54.27
Perovskite/P3HT/WO_3/Ag	J_{SC}	11.35	10.62	10.46	**10.69**	10.40	10.54	8.98	10.89
	V_{OC}	0.87	0.86	0.85	**0.86**	0.88	0.82	0.83	0.84
Type C (□)	PCE	7.77	8.69	7.59	**7.68**	7.26	7.12	6.68	7.54
ITO/PEDOT:PSS/Perovskite/	FF	60.08	79.71	70.80	**75.63**	74.66	77.35	72.19	80.40
PCBM/Ba/Ag	J_{SC}	12.93	10.90	10.72	**10.15**	9.82	9.29	9.35	9.47
	V_{OC}	1.00[a]	1.00[a]	1.00[a]	**1.00**	0.99	0.99	0.99	0.99
Type D (◇)	PCE	3.39	4.88	2.92	**3.72**	3.87	3.92	2.47	4.31
FTO/c-TiO_2/mp-TiO_2/	FF	27.71	38.83	27.13	**38.52**	38.33	41.45	27.42	36.82
mp-Al_2O_3/Graphite	J_{SC}	14.72	14.46	12.99	**10.96**	11.60	11.01	11.12	13.62
	V_{OC}	0.84	0.87	0.83	**0.88**	0.87	0.86	0.81	0.86
Type E (△)[b]	PCE	6.20	10.58	7.07	**9.19**	9.10	10.14	7.98	10.27
ITO/c-TiO_2/Perovskite/	FF	44.33	66.06	48.32	**60.92**	58.08	64.16	52.84	64.16
spiro-OMeTAD/Ag	J_{SC}	13.14	13.27	13.19	**12.76**	13.24	13.08	13.16	13.22
	V_{OC}	0.88	0.99	0.91	**0.97**	0.97	0.99	0.94	1.00
Type F (∗)	PCE	6.08	5.89	5.95	**5.91**	5.51	5.53	5.34	5.38
ITO/c-TiO_2/BCP/	FF	59.03	58.04	58.97	**59.60**	56.90	57.63	56.27	56.43
PTB7:PCBM/PEDOT:PSS/Ag	J_{SC}	11.46	11.42	11.38	**11.34**	11.28	11.17	11.15	11.16
	V_{OC}	0.74	0.73	0.73	**0.72**	0.71	0.71	0.70	0.71

[a]For device Type C, the performed J-V measurement range between 0 and 1 V was insufficient leading to an underestimated V_{OC}.
[b]Device Type E was measured differently with a tracking time of 300 s for MPP, V_{OC}, and J_{SC} tracking, and 1 s resolution for time resolved J-V measurement.

Nevertheless, it is worth mentioning that for certain device architectures (i.e., doped HTL, metal oxide) and measurement conditions (i.e., atmosphere, humidity, temperature) additional effects as light soaking and degradation cannot be excluded. These effects are implied by direct comparison of measurement (I) and (V) (see Table I) and easily verified by long term steady state measurements as seen in Figure S2 of the supplementary material. Therefore, transient measurements, and particularly prolonged time resolved J-V measurements, have to be evaluated carefully as they can be superimposed by such processes. These long-term processes directly compete with long relaxation time scales in the range of tens of seconds as they can occur, i.e., in flat perovskite devices. This prevents reaching a reliable steady state condition in time resolved J-V measurements as the cell is either not completely relaxed or has already changed due to aforementioned effects. As a consequence, it is impractical to extend the measurement time for each individual voltage step without reasonable restrictions or the prior exclusion of such effects. The same applies to the delay time in standard and cyclic J-V measurements. Due to these long-term effects, the cyclic J-V measurement was placed as measurement (III) in the protocol, although it is more reasonable to perform this measurement after the time resolved J-V measurement to verify steady state conditions of extracted time constants. A closer examination of time resolved J-V measurements further reveals a voltage and scan direction dependency of extracted time constants for measured

perovskite solar cells (see Figure S4 of the supplementary material). Thereby, i.e., the device of Type A does not show a significant hysteresis and a small time dependence up to the maximum power point, whereas the time dependence becomes more evident and the corresponding relaxation times increase approaching the V_{OC}. In contrast, Type B and C devices show the most pronounced time dependence at the maximum power point, which is decreasing towards the J_{SC} and V_{OC}.

In summary, only stabilized results represent realistic values for the efficiency of a solar cell in operation. Thereby, quickly degrading solar cells are easily revealed by the tracking algorithm and have to be reviewed prior to publication, whereas cells showing a pronounced light soaking effect first have to be settled to reach steady state working conditions. J-V measurements, whether time-resolved or not, cannot provide such reliable steady state conditions for all device architectures and can differ significantly from device characteristics extracted from stabilized measurements. Finally, even time constants extracted from time resolved measurements cannot always reveal necessary measurement requirements to reach steady state conditions, as these relaxation times can either exceed feasible measurement durations or vary with applied voltage.

As a measurement protocol for reliable performance determination of perovskite solar cells, we propose as only reproducible method the stabilization of the maximum power point, the actual working condition of a solar cell. Therefore, a tracking algorithm is more reliable than a simple transient current measurement for a specific voltage, as the maximum power point can change due to the relaxation process in perovskite as well as the aforementioned light soaking and degradation effects. Additional characteristics as J_{SC} and V_{OC} have to be extracted likewise from stabilized measurements resulting in a stabilized fill factor. Thus, for reproducibility and comparability, J-V measurements should always include stabilized device characteristics, even for hysteresis free devices at a first glance. Finally, further insight on processes and time scales occurring in fabricated devices can be obtained by time resolved as well as cyclic J-V measurements.

For detailed information about characterization methods, and the technical implementation of the algorithms see the supplementary material.

See the supplementary material for device preparation methods, detailed explanation of the tracking algorithm, and additional measurements.

We acknowledge the funding from the German Federal Ministry of Education and Research (BMBF, project MesoPIN), the Baden-Württemberg Foundation for the project "BioMat-S7: SUPERSOL" in the program "Biomimetic Materials Synthesis," and the REFINE research consortium funded by the Carl Zeiss Foundation.

[1] A. Kojima *et al.*, "Organometal halide perovskites as visible-light sensitizers for photovoltaic cells," J. Am. Chem. Soc. **131**(17), 6050–6051 (2009).
[2] M. M. Lee *et al.*, "Efficient hybrid solar cells based on meso-superstructured organometal halide perovskites," Science **338**(6107), 643–647 (2012).
[3] H. S. Kim *et al.*, "Lead iodide perovskite sensitized all-solid-state submicron thin film mesoscopic solar cell with efficiency exceeding 9%," Sci. Rep. **2**, 591 (2012).
[4] N. J. Jeon *et al.*, "Compositional engineering of perovskite materials for high-performance solar cells," Nature **517**(7535), 476–480 (2015).
[5] W. S. Yang *et al.*, "High-performance photovoltaic perovskite layers fabricated through intramolecular exchange," Science **348**(6240), 1234–1237 (2015).
[6] D. Wang *et al.*, "Stability of perovskite solar cells," Sol. Energy Mater. Sol. Cells **147**, 255–275 (2016).
[7] N. Ahn *et al.*, "Highly reproducible perovskite solar cells with average efficiency of 18.3% and best efficiency of 19.7% fabricated via Lewis base adduct of lead (II) iodide," J. Am. Chem. Soc. **137**(27), 8696–8699 (2015).
[8] Z. Yang *et al.*, "An up-scalable approach to $CH_3NH_3PbI_3$ compact films for high-performance perovskite solar cells," Nano Energy **15**, 670–678 (2015).
[9] T. P. Gujar and M. Thelakkat, "Highly reproducible and efficient perovskite solar cells with extraordinary stability from robust $CH_3NH_3PbI_3$: Towards large-area devices," Energy Technol. **4**(3), 449–457 (2016).
[10] H. J. Snaith *et al.*, "Anomalous hysteresis in perovskite solar cells," J. Phys. Chem. Lett. **5**(9), 1511–1515 (2014).
[11] W. Tress *et al.*, "Understanding the rate-dependent J-V hysteresis, slow time component, and aging in $CH_3NH_3PbI_3$ perovskite solar cells: The role of a compensated electric field," Energy Environ. Sci. **8**(3), 995–1004 (2015).
[12] A. Hinsch *et al.*, "Status of dye solar cell technology as a guideline for further research," ChemPhysChem **15**(6), 1076–1087 (2014).
[13] J. Burschka *et al.*, "Sequential deposition as a route to high-performance perovskite-sensitized solar cells," Nature **499**(7458), 316–319 (2013).
[14] M. Liu, M. B. Johnston, and H. J. Snaith, "Efficient planar heterojunction perovskite solar cells by vapour deposition," Nature **501**(7467), 395–398 (2013).

[15] C. W. Chen *et al.*, "Efficient and uniform planar-type perovskite solar cells by simple sequential vacuum deposition," Adv. Mater. **26**(38), 6647–6652 (2014).
[16] N. J. Jeon *et al.*, "Solvent engineering for high-performance inorganic-organic hybrid perovskite solar cells," Nat. Mater. **13**(9), 897–903 (2014).
[17] F. X. Xie *et al.*, "Vacuum-assisted thermal annealing of $CH_3NH_3PbI_3$ for highly stable and efficient perovskite solar cells," ACS Nano **9**(1), 639–646 (2015).
[18] H. Hu *et al.*, "Highly efficient reproducible perovskite solar cells prepared by low-temperature processing," Molecules **21**(4), 542–552 (2016).
[19] A. Abrusci *et al.*, "High-performance perovskite-polymer hybrid solar cells via electronic coupling with fullerene monolayers," Nano Lett. **13**(7), 3124–3128 (2013).
[20] O. Malinkiewicz *et al.*, "Perovskite solar cells employing organic charge-transport layers," Nat. Photonics **8**(2), 128–132 (2014).
[21] S. Meloni *et al.*, "Ionic polarization-induced current-voltage hysteresis in $CH_3NH_3PbX_3$ perovskite solar cells," Nat. Commun. **7**, 10334 (2016).
[22] E. L. Unger *et al.*, "Hysteresis and transient behavior in current-voltage measurements of hybrid-perovskite absorber solar cells," Energy Environ. Sci. **7**(11), 3690–3698 (2014).
[23] H. S. Kim and N. G. Park, "Parameters affecting I-V hysteresis of $CH_3NH_3PbI_3$ perovskite solar cells: Effects of perovskite crystal size and mesoporous TiO_2 layer," J. Phys. Chem. Lett. **5**(17), 2927–2934 (2014).
[24] J. C. Yu *et al.*, "High-performance planar perovskite optoelectronic devices: A morphological and interfacial control by polar solvent treatment," Adv. Mater. **27**(23), 3492–3500 (2015).
[25] J. M. Frost *et al.*, "Atomistic origins of high-performance in hybrid halide perovskite solar cells," Nano Lett. **14**(5), 2584–2590 (2014).
[26] J. M. Frost, K. T. Butler, and A. Walsh, "Molecular ferroelectric contributions to anomalous hysteresis in hybrid perovskite solar cells," APL Mater. **2**(8), 081506 (2014).
[27] Y. Kutes *et al.*, "Direct observation of ferroelectric domains in solution-processed $CH_3NH_3PbI_3$ perovskite thin films," J. Phys. Chem. Lett. **5**(19), 3335–3339 (2014).
[28] M. Christoforo *et al.*, "Transient response of organo-metal-halide solar cells analyzed by time-resolved current-voltage measurements," Photonics **2**(4), 1101–1115 (2015).
[29] H. S. Kim *et al.*, "Control of I-V hysteresis in $CH_3NH_3PbI_3$ perovskite solar cell," J. Phys. Chem. Lett. **6**(22), 4633–4639 (2015).
[30] Y. Shao *et al.*, "Origin and elimination of photocurrent hysteresis by fullerene passivation in $CH_3NH_3PbI_3$ planar heterojunction solar cells," Nat. Commun. **5**, 5784 (2014).
[31] C. G. Wu *et al.*, "High efficiency stable inverted perovskite solar cells without current hysteresis," Energy Environ. Sci. **8**(9), 2725–2733 (2015).
[32] W. Nie *et al.*, "Solar cells. High-efficiency solution-processed perovskite solar cells with millimeter-scale grains," Science **347**(6221), 522–525 (2015).
[33] N. Tripathi *et al.*, "Hysteresis-free and highly stable perovskite solar cells produced via a chlorine-mediated interdiffusion method," J. Mater. Chem. A **3**(22), 12081–12088 (2015).
[34] J. A. Christians, J. S. Manser, and P. V. Kamat, "Best practices in perovskite solar cell efficiency measurements. Avoiding the error of making bad cells look good," J. Phys. Chem. Lett. **6**(5), 852–857 (2015).
[35] H. Yu *et al.*, "Native defect-induced hysteresis behavior in organolead iodide perovskite solar cells," Adv. Funct. Mater. **26**(9), 1411–1419 (2016).
[36] Y. Hishikawa *et al.*, "Precise performance characterization of perovskite solar cells," Curr. Appl. Phys. **16**(8), 898–904 (2016).
[37] R. Roesch *et al.*, "Procedures and practices for evaluating thin-film solar cell stability," Adv. Energy Mater. **5**(20), 1501407 (2015).
[38] E. Zimmermann, GitHub Repository of Eugen Zimmermann, 2016, available from: https://github.com/EugenZimmermann/matlab-keithley-jv.
[39] J. A. Christians, P. A. Miranda Herrera, and P. V. Kamat, "Transformation of the excited state and photovoltaic efficiency of $CH_3NH_3PbI_3$ perovskite upon controlled exposure to humidified air," J. Am. Chem. Soc. **137**(4), 1530–1538 (2015).
[40] K.-D. Kim *et al.*, "Decoupling optical and electronic optimization of organic solar cells using high-performance temperature-stable TiO_2/Ag/TiO_2 electrodes," APL Mater. **3**(10), 106105 (2015).